Humble planar defects in SiGe nanopillars

Hongbin Yang [1,*] Shang Ren [2] Sobhit Singh [2,3] Emily M. Turner [4] Kevin S. Jones,[4] Philip E. Batson [2] David Vanderbilt [2] and Eric Garfunkel[1,2,†]

[1]*Department of Chemistry and Chemical Biology, Rutgers University, Piscataway, New Jersey 08854, USA*
[2]*Department of Physics and Astronomy, Rutgers University, Piscataway, New Jersey 08854, USA*
[3]*Department of Mechanical Engineering, University of Rochester, Rochester, New York 14627, USA*
[4]*Department of Material Science and Engineering, University of Florida, Gainesville, Florida 32611, USA*

(Received 31 October 2021; accepted 9 August 2022; published 31 August 2022)

We report a {001} planar defect found in SiGe nanopillars. The defect structure, determined by atomic-resolution electron microscopy, matches the Humble defect model proposed for diamond. We also investigate several possible variants of the Humble structure using first-principles calculations and find that the one lowest in energy is in agreement with the scanning transmission electron microscope images. The pillar composition has been analyzed with electron energy loss spectroscopy, which hints at how the defect is formed. Our results show that the structure and formation process of defects in nanostructured group IV semiconductors can be different from their bulk counterparts.

DOI: 10.1103/PhysRevB.106.054114

I. INTRODUCTION

Group IV semiconductors containing Si and Ge are ubiquitous in today's electronics devices [1]. Some of these materials also have promising characteristics for applications in quantum information processing [2,3]. Defects in these diamond cubic crystals may influence their properties in device applications, which is one key reason for the extensive study of their structure and formation process. One set of the most widely studied defects are the {001} planar defects in natural diamond [4]. Many structural models have been proposed in order to find a match with experiments. Among many other models [5,6], Humble proposed a planar defect that can be regarded as resulting from the insertion of an entire layer of fourfold coordinated interstitial carbon atoms [7]. Humble defects in Si have also attracted attention. Arai *et al.* theoretically studied the self-interstitials in Si and found that defect formation with a Humble structure lowers the total energy significantly compared to free interstitials [8]. Goss *et al.* further studied the bonding configuration of the Humble defect and proposed four other variations, and also calculated their energies, for both C and Si [9–11].

Experimentally, {001} planar defects are often observed in Si and Ge after H implantation [12,13]. In ultrafast laser-annealed ion-implanted Si samples, defects in {001} planes appear as self-interstitial loops [14,15]. Under thermal equilibrium, planar defects in Si and SiGe are primarily found along the {113} planes, and occasionally in {111} planes [16]. Despite a large number of observations and calculations for defects in Si and Ge, the defect structure, preferred plane, and dimension are still not fully predictable. For the defects that have been observed earlier, only a few of them have been examined by atomic-resolution high angle annular dark field (HAADF) imaging, which allows a direct and quantitative comparison with computationally predicted structures [17]. In a recent electron microscopy study of planar defects in diamond, it was clearly shown that {001} platelet defects do not adopt the Humble structure [4]. Interestingly, the Humble structure can describe a {001} planar defect found in Ge [18]. In Si, however, there is no clear evidence of Humble defects in experiments. A number of calculations found that {001}- and {113}-oriented defects in Si have similar energies [10,19,20].

While bulk group IV materials and their defects have been extensively studied for decades, nanostructures of these materials are a subject of active research for their new and potentially useful electronic and optical properties [21–25]. During the growth or fabrication of these nanostructures, new structural phases and defects are occasionally encountered [26–30]. The deliberate placement of defects in the nanostructures may offer yet another knob to tune properties or to create new classes of devices.

In this paper, we report an experimental observation of Humble defects in $Si_{0.2}Ge_{0.8}$ (hereafter referred to as SiGe). We have investigated the atomic structure of this defect by HAADF imaging in an aberration-corrected scanning transmission electron microscope (STEM). The defect structure and atomic coordinates in experiments are in good agreement with density functional theory (DFT) calculations. The local Si percentage and electronic structure across the defect have also been studied with high-resolution electron energy loss spectroscopy (EELS), which provides information on how these defects are formed.

II. RESULT AND DISCUSSION

The defects we study in this paper are observed in SiGe nanopillars, which were formed by the oxidation of Si/SiGe superlattices that are patterned into cylindrical rods [31].

*hongbin.yang@rutgers.edu
†egarf@chem.rutgers.edu

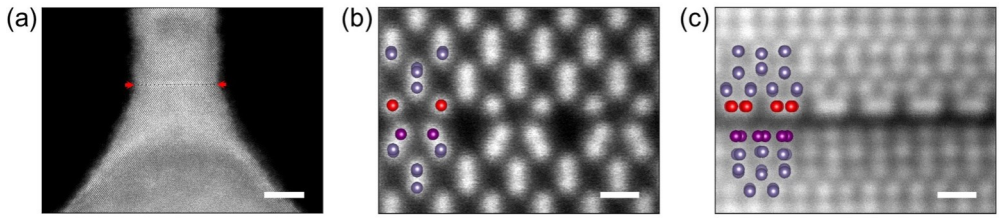

FIG. 1. Atomic structure of the SiGe Humble defect. (a) Low-magnification HAADF-STEM images of the SiGe pillar. Scale bar: 10 nm. The planar defect in this pillar is indicated by the two red arrows. (b) Atomic-resolution HAADF-STEM images of the defect viewed from [110] projection, and (c) from [210] projection, with the structural models shown superimposed. Scale bar: 3 Å.

Oxidations were done under dry O_2 at 900 °C for 20 min. Oxidation of SiGe results first in the formation of SiO_2, as Ge oxides are much less stable than SiO_2. When the desired oxidation time is reached, the wafer was quenched to room temperature within 1 min. A transmission electron microscopy lamella was extracted by a focused ion beam lift-out process. We then remove the oxides by hydrofluo-ric acid etching [32]. The remaining partially oxidized SiGe pillar was subsequently studied in this paper using a Nion UltraSTEM 100 aberration-corrected scanning transmission electron microscope.

One image of a SiGe pillar is shown in shown in Fig. 1(a), where a planar defect forms parallel to the wafer surface; the defect appears uniform across this 17-nm-diameter pillar, and in many other similar pillars. Atomic-resolution imaging of this defect has been carried out in our STEM operating at 60 kV, below the damage threshold [16]. Atomic-resolution HAADF images of the defect from two directions are shown in Figs. 1(b) and 1(c). These images allow us to determine the defect structure and compare it with structural models proposed earlier for other group IV materials and structures.

For an extended two-dimensional (2D) Humble defect, the atomic arrangement at the defect core is not unique. Goss *et al.* proposed several variations of the original Humble configurations. Figure 2 shows all of these models as viewed from three major axes [33]. The difference between these models primarily stems from the two layers of atoms shown in red and purple, which we will refer to as the defect core in the rest of this paper. Either the red or the purple layer can be considered as a layer of interstitial atoms, whose removal could result in a perfect bulk lattice. The atoms at the defect core form bonds within the *a-b* plane, but with nearest neighbors in different directions, as can be seen from the [001] view in Fig. 2. Within these models, all atoms in both the bulk and defect core are fourfold coordinated. The different bonding configuration at the defect core leads to large distortions in bond angles, different from the perfect tetragonal bonding geometry in an ideal bulk diamond cubic lattice, where all the bond angles are 109.5°.

To identify which of these variants of the Humble defect are present in our sample, we start with a preliminary screening of their energies using DFT calculations. For this purpose, the formation energies of various Humble defect models are calculated using DFT. A nine-layer tetragonal unit cell is found to be sufficient in our calculations to capture the essential structural and energetic properties. In this work, all DFT calculations are performed using the Vienna *ab initio* simulation package (VASP) [34] and the projector augmented-wave (PAW) [35,36] method with Ge $4s^2 4p^2$ and Si $4s^2 4p^2$ pseudopotential valence configurations. The exchange correlation used is the generalized-gradient approximation (GGA) as parametrized by Perdew, Burke, and Ernzerhof (PBE) [37]. The relaxation of the nine-layer Humble A structure is performed with a 6 × 6 × 4 Monkhorst-Pack [38] *k* mesh, and

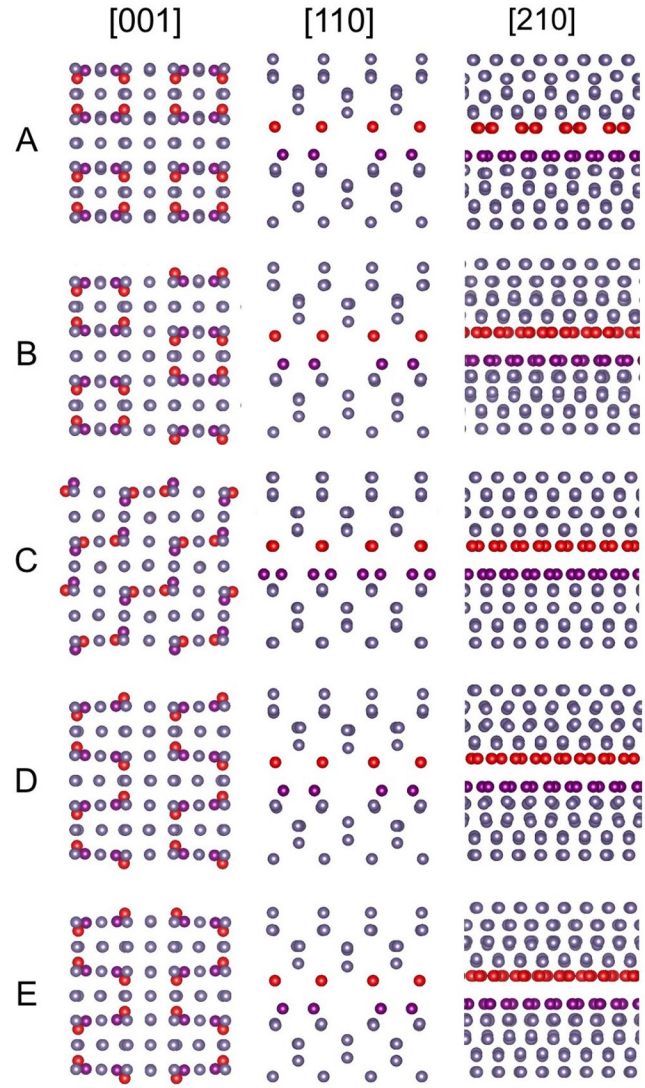

FIG. 2. Structural models of the five Humble defects proposed by Goss *et al.* viewed from the [001], [110], and [210] axes, defined relative to the bulk lattice. Atoms shown in red and purple indicate the upper and lower atoms that are under significant bond angle distortion.

TABLE I. DFT-calculated formation energy (eV/interstitial) for the five Humble models in pure Ge and $Si_{0.2}Ge_{0.8}$.

Models	A	B	C	D	E
Ge	0.309	0.354	0.422	0.363	0.360
SiGe	0.297	0.342	0.411	0.351	0.350

a corresponding k mesh is used for the relaxation of Humble A–E structures. The in-plane lattice constants are fixed to the DFT relaxed value for bulk SiGe (8.16 Å, $\sqrt{2}a_{SiGe}$), and only the c lattice constant is relaxed. The convergence criteria for forces and energies are 10^{-3} eV/Å and 10^{-7} eV, respectively, and the cutoff energy for the plane-wave basis is 500 eV. The virtual crystal approximation (VCA) [39] is used when simulating Humble defects in the $Si_{0.2}Ge_{0.8}$ alloy. In this approach, all atoms are identical, with each being a 20%–80% weighted average of Si and Ge character. Although absolute values from VCA may not be accurate, relative energies between the defect structures computed within VCA should be correct.

All structural models in Fig. 2 show a relatively low formation energy, as shown in Table I. These results suggest that model A has the lowest energy in the case of both pure Ge and $Si_{0.2}Ge_{0.8}$. The formation energy of the {001} Humble defect in pure Si is 0.45 eV per interstitial [10], higher than those in pure Ge or Ge-rich SiGe (Table I), suggesting that forming {001} Humble defects in pure Si is energetically less favorable. However, the formation energies of the {001} Humble defects in diamond are an order of magnitude higher than our results [11]. This may explain why Humble defects are only observed in SiGe or Ge but not in Si or C.

Next, we turn to a more complete determination of the defect structure based on STEM imaging and DFT calculations. Despite having different atomic structures, models A, B, D, and E are almost identical when viewed from the [110] direction. Therefore, imaging only from [110] (the most commonly imaged axis for a diamond cubic crystal) is not sufficient to determine the defect atomic structure. As shown in Figs. 1(b) and 2, we see five- and eight-member rings at the defect. The lower half of the defect resembles the symmetric dimers of a 2 × 1 reconstructed (001) surface of Si. To fully understand the atomic arrangements at the defect core, the defect has also been imaged along the [210] projection. This is done by tilting the specimen so that the pillar rotates along the c axis 26.6° away from [110] projection. The corresponding image is shown in Fig. 1(c), where the upper layer of the defect core appears as dumbbells of atomic columns. Comparing the HAADF intensities with simulated ones from the DFT-relaxed structure models in Fig. 3(a), we see that model A yields the best match with experiments. Within each dumbbell, the two atomic columns are separated by 115 pm, and the distance between the dumbbells is 363 pm. The subtle differences between models B, D, and E in their [210] view are too small to differentiate. Therefore, we only simulate the HAADF intensity from model D to compare with experiment. We find that they show equally spaced atomic columns that are separated by 180 pm, which does not match with what we observe in experiments. The lower layers of the defect core (purple atoms in Figs. 1(b), 1(c), and 2) in all models show

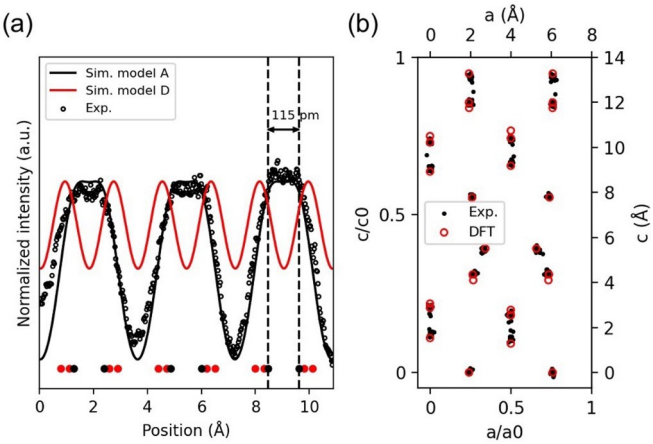

FIG. 3. Experimental defect structure compared with DFT-calculated ones. (a) HAADF intensity profiles of the HAADF image in Fig. 1(b) for the upper layer of the defect core compared with simulated ones from Humble models A and D. DFT-calculated atomic coordinates are shown as black and red dots for models A and D, respectively, at the bottom. (b) Experimental atomic coordinates from 2D Gaussian fitting of the HAADF images in Fig. 1 compared with DFT-relaxed Humble model A.

atomic columns that are separated by either 40 or 56 pm, and therefore are observed as single atomic columns in Fig. 1(c) and cannot be used to distinguish between models B, D, and E.

A more quantitative comparison between experiment and theory is shown in Fig. 3(b). From the HAADF images in Fig. 1, we extract atomic positions by 2D Gaussian fitting for each of the atomic columns. The fitting results are shown in Fig. 3(b), which overall match with the DFT-relaxed atomic coordinates, although some subtle differences do exist (i.e., the bond distances in the purple layer are slightly larger in the experiment than calculated by DFT). We also see that even the atoms that are one layer away from the defect core show modulation in the c-axis direction. This shift is observed both in experiment and theory.

By combining atomic-resolution ADF imaging with DFT calculations, we have completely determined the defect structure. We conclude that the symmetry of the original Humble defect (model A) applies to the one reported here in SiGe, and that atomic coordinates of the DFT-relaxed structure match well with the experimental results. This defect is equivalent in its [110] and [110] views, both of which are observed in the HAADF image in Fig. 4, where the upper and lower layers of the defect core alternate in the a-b plane. In addition to this predominant defect that we observe in many pillars, we also note that {001} defects with a different structure than model A, and even a {113} defect, have also been observed, but much less frequently (only in one pillar).

As mentioned earlier, the defects are formed after the oxidation of Si/SiGe nanopillars. This process is unusual and different from earlier works on planar defects in Si and Ge, in which the defect creation process usually involved ion implantation or high-energy electron irradiation [16,18]. The creation and diffusion of point defects, such as interstitials and vacancies, are often responsible for the formation of extended defects.

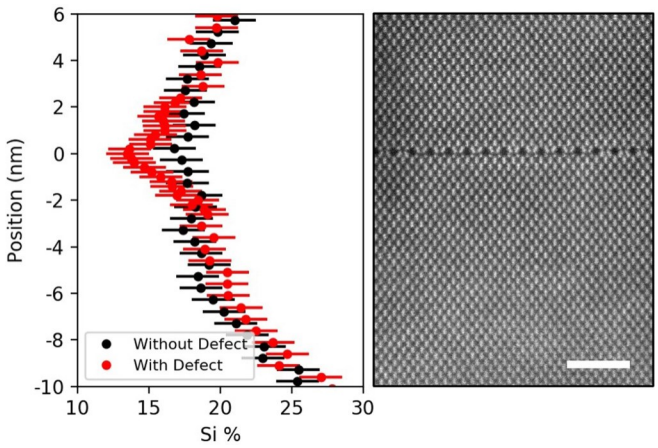

FIG. 4. Si percentage of SiGe pillars near the Humble defect. EELS line profiles of Si content across the defect in the area shown on the right. Same information for a SiGe pillar without the defect is shown in comparison. Scale bar: 2 nm.

The Si percentage of the SiGe layer in the pillar has been quantified by EELS in Fig. 4, which drops by about 10% to 20% after oxidation, and the initially sharp Si/SiGe interface becomes one with the graded Si percentage. Very close to the defect, we see a further decrease in Si content to lower than 20%. The lowered Si content at the defect core also suggests that the defect occurs with predominantly Ge-Ge bonding. The tendency of having less Si at the defect core is also supported by DFT calculations. When substituting one Si atom into the 13-layer Humble unit cell made of Ge, the layer-averaged formation energy is highest at the defect core, suggesting it is the least preferred location for a Si substitution.

Based on the SiGe pillar composition before and after oxidation, and the knowledge that the planar defect observed has a lower atomic density than the bulk lattice, we propose the following mechanism to explain the defect formation based on thermodynamic and kinetic reasoning. During high-temperature oxidation, the high stability of silicon oxide relative to germanium oxide leads to an effective out-diffusion of Si, lowering the Si concentration in the SiGe nanostructure. The Si out-diffusion leads to vacancy formation, some of which is annihilated by shrinking of the structure, but some of which remains. Vacancies can then diffuse and aggregate to form planar defects which are lower in energy than an equivalent number of randomly placed vacancies. Ge at the planar defect has a lower energy than Si, thus the local change in Si percentage. In previous literature [7,8], similar defects were constructed by adding one extra layer of atoms, and were referred to as interstitials instead of vacancies. Regardless of the term used, we note that the atomic density is lower at the defect than in the bulk.

Moreover, we note that although there are several alternating layers of SiGe/Si on the Si substrate, the Humble defects were only found in the middle of the first SiGe layer after oxidation, and at a fixed distance to the Si substrate surface. The location of the planar defect in the nanostructure may be the result of either diffusion kinetics (more probable for vacancies to diffuse to the middle of the structure) or energetics (the strain energy of a planar defect is lowest in the nanostructure where the defect is observed). Further studies on the pillar size, oxidation condition, and alloy concentration dependence of such defects would be required to verify and quantify this or alternative mechanisms.

The electronic structure of this defect has been investigated by high-resolution electron energy loss spectroscopy and density functional theory, and will be reported elsewhere [40].

III. CONCLUSIONS

In summary, we found that {001} Humble planar defects can form in SiGe nanopillars after dry oxidation and quenching. By combining atomic-resolution electron microscopy and first-principles calculations, the defect structure, composition, and energetics have been studied in detail, and compared with previous studies on other group IV semiconductors. Future study of the compositional, pillar size, and processing condition dependence of the Humble defect will provide further insight into the formation mechanism.

ACKNOWLEDGMENTS

H.Y. and E.G. acknowledge the financial support from the U.S. Department of Energy, under Award No. DE-EE0008083. S.R. and D.V. are supported by NSF Grant No. DMR-1954856. S.S. acknowledges the support from the U.S. Department of Energy (DOE), Office of Science, Basic Energy Sciences under Award No. DESC0020353.

[1] D. J. Paul, Semicond. Sci. Technol. **19**, R75 (2004).
[2] G. Scappucci, C. Kloeffel, F. A. Zwanenburg, D. Loss, M. Myronov, J.-J. Zhang, S. De Franceschi, G. Katsaros, and M. Veldhorst, Nat. Rev. Mater. **6**, 926 (2021).
[3] N. P. de Leon, K. M. Itoh, D. Kim, K. K. Mehta, T. E. Northup, H. Paik, B. S. Palmer, N. Samarth, S. Sangtawesin, and D. W. Steuerman, Science **372**, eabb2823 (2021).
[4] E. J. Olivier, J. H. Neethling, R. E. Kroon, S. R. Naidoo, C. S. Allen, H. Sawada, P. A. van Aken, and A. I. Kirkland, Nat. Mater. **17**, 243 (2018).
[5] A. R. Lang, Proc. Phys. Soc. **84**, 871 (1964).
[6] C. R. Miranda, A. Antonelli, and R. W. Nunes, Phys. Rev. Lett. **93**, 265502 (2004).
[7] P. Humble and P. B. Hirsch, Proc. R. Soc. London, Ser. A **381**, 65 (1982).
[8] N. Arai, S. Takeda, and M. Kohyama, Phys. Rev. Lett. **78**, 4265 (1997).
[9] J. P. Goss, B. J. Coomer, R. Jones, T. D. Shaw, P. R. Briddon, M. Rayson, and S. Öberg, Phys. Rev. B **63**, 195208 (2001).
[10] J. P. Goss, T. A. G. Eberlein, R. Jones, N. Pinho, A. T. Blumenau, T. Frauenheim, P. R. Briddon, and S. Öberg, J. Phys.: Condens. Matter **14**, 12843 (2002).

[11] J. P. Goss, B. J. Coomer, R. Jones, C. J. Fall, P. R. Briddon, and S. Öberg, Phys. Rev. B **67**, 165208 (2003).
[12] M. L. David, F. Pailloux, D. Babonneau, M. Drouet, J. F. Barbot, E. Simoen, and C. Claeys, J. Appl. Phys. **102**, 096101 (2007).
[13] T. Akatsu, K. K. Bourdelle, C. Richtarch, B. Faure, and F. Letertre, Appl. Phys. Lett. **86**, 181910 (2005).
[14] L. A. Marqués, M. Aboy, I. Santos, P. López, F. Cristiano, A. La Magna, K. Huet, T. Tabata, and L. Pelaz, Phys. Rev. Lett. **119**, 205503 (2017).
[15] Y. Qiu, F. Cristiano, K. Huet, F. Mazzamuto, G. Fisicaro, A. La Magna, M. Quillec, N. Cherkashin, H. Wang, S. Duguay, and D. Blavette, Nano Lett. **14**, 1769 (2014).
[16] L. Fedina, O. I. Lebedev, G. Van Tendeloo, J. Van Landuyt, O. A. Mironov, and E. H. C. Parker, Phys. Rev. B **61**, 10336 (2000).
[17] K. J. Dudeck, L. A. Marqués, A. P. Knights, R. M. Gwilliam, and G. A. Botton, Phys. Rev. Lett. **110**, 166102 (2013).
[18] S. Muto and S. Takeda, Philos. Mag. Lett. **72**, 99 (1995).
[19] S. S. Kapur and T. Sinno, Phys. Rev. B **82**, 045205 (2010).
[20] S. S. Kapur, A. M. Nieves, and T. Sinno, Phys. Rev. B **82**, 045206 (2010).
[21] G. H. Zhu, H. Lee, Y. C. Lan, X. W. Wang, G. Joshi, D. Z. Wang, J. Yang, D. Vashaee, H. Guilbert, A. Pillitteri, M. S. Dresselhaus, G. Chen, and Z. F. Ren, Phys. Rev. Lett. **102**, 196803 (2009).
[22] S. K. Bux, R. G. Blair, P. K. Gogna, H. Lee, G. Chen, M. S. Dresselhaus, R. B. Kaner, and J.-P. Fleurial, Adv. Funct. Mater. **19**, 2445 (2009).
[23] T.-L. Chan and J. R. Chelikowsky, Nano Lett. **10**, 821 (2010).
[24] W. M. Brewer, Y. Xin, C. Hatem, D. Diercks, V. Q. Truong, and K. S. Jones, Nano Lett. **17**, 2159 (2017).
[25] E. M. T. Fadaly, A. Dijkstra, J. R. Suckert, D. Ziss, M. A. J. van Tilburg, C. Mao, Y. Ren, V. T. van Lange, K. Korzun, S. Kölling, M. A. Verheijen, D. Busse, C. Rödl, J. Furthmüller, F. Bechstedt, J. Stangl, J. J. Finley, S. Botti, J. E. M. Haverkort, and E. P. A. M. Bakkers, Nature (London) **580**, 205 (2020).
[26] Y. Qiu, H. Bender, O. Richard, M. S. Kim, E. Van Besien, I. Vos, M. de Potter de ten Broeck, D. Mocuta, and W. Vandervorst, Sci. Rep. **5**, 12692 (2015).
[27] G. Dushaq, A. Nayfeh, and M. Rasras, Sci. Rep. **9**, 1593 (2019).
[28] A. V. Kozhemiako, A. P. Evseev, Y. V. Balakshin, and A. A. Shemukhin, Semiconductors **53**, 800 (2019).
[29] C. Bradac, W. Gao, J. Forneris, M. E. Trusheim, and I. Aharonovich, Nat. Commun. **10**, 5625 (2019).
[30] E. M. T. Fadaly, A. Marzegalli, Y. Ren, L. Sun, A. Dijkstra, D. de Matteis, E. Scalise, A. Sarikov, M. De Luca, R. Rurali, I. Zardo, J. E. M. Haverkort, S. Botti, L. Miglio, E. P. A. M. Bakkers, and M. A. Verheijen, Nano Lett. **21**, 3619 (2021).
[31] E. M. Turner, Q. Campbell, J. Pizarro, H. Yang, K. R. Sapkota, P. Lu, A. D. Baczewski, G. T. Wang, and K. S. Jones, Nano Lett. **21**, 7905 (2021).
[32] E. M. Turner, K. R. Sapkota, C. Hatem, P. Lu, G. T. Wang, and K. S. Jones, Ultramicroscopy **216**, 113049 (2020).
[33] K. Momma and F. Izumi, J. Appl. Crystallogr. **44**, 1272 (2011).
[34] G. Kresse and J. Furthmüller, Phys. Rev. B **54**, 11169 (1996).
[35] P. E. Blöchl, Phys. Rev. B **50**, 17953 (1994).
[36] G. Kresse and D. Joubert, Phys. Rev. B **59**, 1758 (1999).
[37] J. P. Perdew, K. Burke, and M. Ernzerhof, Phys. Rev. Lett. **77**, 3865 (1996).
[38] H. J. Monkhorst and J. D. Pack, Phys. Rev. B **13**, 5188 (1976).
[39] L. Bellaiche and D. Vanderbilt, Phys. Rev. B **61**, 7877 (2000).
[40] S. Ren, H. Yang, S. Singh, P. E. Batson, E. L. Garfunkel, and D. Vanderbilt, arXiv:2206.13726 (2022).